# Scroll waves in spherical shell geometries

Francisco Chávez and Raymond Kapral
*Chemical Physics Theory Group, Department of Chemistry, University of Toronto, Ontario M5S 3H6, Canada*

Guillaume Rousseau
*Groupe SYRRA, case 7008, UFR de Physique, Université Denis Diderot, 2 place Jussieu, 75251 Paris Cedex 05, France*

Leon Glass
*Department of Physiology, McGill University, Montreal, Quebec H3G 1Y6, Canada*

(Received 25 April 2001; accepted 21 July 2001; published 4 October 2001)

The evolution of scroll waves in excitable media with spherical shell geometries is studied as a function of shell thickness and outer radius. The motion of scroll wave filaments that are the locii of phaseless points in the medium and organize the wave pattern is investigated. When the inner radius is sufficiently large the filaments remain attached to both the inner and outer surfaces. The minimum size of the sphere that supports spiral waves and the maximum number of spiral waves that can be sustained on a sphere of given size are determined for both regular and random initial distributions. When the inner radius is too small to support spiral waves the filaments detach from the inner surface and form a curved filament connecting the two spiral tips in the surface. In certain parameter domains the filament is an arc of a circle that shrinks with constant shape. For parameter values close to the meandering border, the filament grows and collisions with the sphere walls lead to turbulent filament dynamics. © *2001 American Institute of Physics.* [DOI: 10.1063/1.1406537]

**Geometry often plays a role in determining the nature of pattern structure and dynamics. Our interest is in excitable systems where wave propagation may be strongly influenced by geometrical features. Such systems are common in nature and the propagation of electrochemical waves in the heart is an especially important example. It is known that factors such as the topology, thickness, and inhomogeniety of cardiac tissue can strongly influence wave propagation and give rise to fibrillation or flutter. In this paper we do not consider such complex systems but instead examine the much simpler case of excitable media with spherical shell geometries. For this highly idealized case we are able to study in quantitative detail the effects of geometry on the nature of the wave propagation processes. The work provides insight into some of the geometrical factors that determine wave dynamics which may be relevant for more complicated systems.**

## I. INTRODUCTION

Spiral waves are one of the most commonly found patterns in chemical and biological excitable media. Spiral and scroll waves have been studied extensively in chemically reacting media such as the Belousov–Zhabotinsky (BZ) system in a variety of two- and three-dimensional geometries.[1] In biological systems they play an important role in processes like dictyostelium discoideum aggregation and movement, $Ca^{2+}$ wave propagation in xenopus oocytes and other contexts,[2] and electrochemical wave propagation in the heart.[3,4] In many of these examples the geometry in which the spiral wave dynamics takes place is complex and the nature of the dynamics depends on the geometry in a nontrivial manner. The focus of this study is on the effects of geometry on scroll wave dynamics.

One of our motivations for studying this problem is to develop a theoretical basis for understanding the dynamics of cardiac arrhythmias which are abnormal rhythms in the heart. In normal hearts cardiac arrhythmias are rare, but in diseased hearts cardiac arrhythmias can become more common. For example, if chambers of the heart become abnormally large, they are susceptible to serious arrhythmias in which waves are believed to circulate in a fashion that is similar to the circulation of the BZ waves in a chemical medium. Although such arrhythmias are most likely associated with changes both in the physiological properties (this translates into the associated nonlinear kinetics in reaction diffusion models of cardiac propagation) of the tissue as well as the geometry of the tissue, abnormal heart geometries confer significant risk for serious arrhythmia.[5] For instance, therapies that target specific anatomical regions of the heart for radio-frequency ablation often owe their success to the destruction of anatomical features that are necessary either for sustaining or initiating arrhythmia. Thus, it becomes immediately of interest to investigate the possible types of wave organization and their dynamics as a function of the geometry of the excitable medium in which waves propagate. Real human hearts are enormously complex three-dimensional structures. Although there have been investigations of the dynamics in these complex geometrical domains,[6] in the current study we investigate propagation in an extremely simple geometry—a spherical shell. Even this problem presents challenges and its complete solution is lacking.

 

There have been theoretical studies of a pair of counter-rotating spiral waves whose tips are located at opposite poles of a spherical surface.[7–9] A class of asymmetric counter-rotating spiral waves on the surface of a sphere has been studied using the eikonal approximation.[10] Numerical solutions of the reaction–diffusion equations on spherical geometries have been used to study the dynamics of a spiral wave pair.[11] More complicated, even chaotic, behavior was found in numerical studies in inhomogeneous media with a spherical geometry.[12] Spiral wave patterns have also been observed in experiments on the BZ reaction on spherical beads.[13]

Our investigations of scroll waves in spherical shell geometries are organized as follows: Section II describes the evolution of scroll wave pairs in the FitzHugh–Nagumo system as a function of the thickness of the spherical shell for a fixed value of the outer radius of the surface. Section III is devoted to an investigation of the maximum number of spiral waves that a thin spherical shell can support starting both from regular and random initial conditions. The case of scroll wave filament evolution in solid spheres is the topic of Sec. IV where parameter values leading both to filament shrinkage and turbulence are studied. The conclusions of the study are presented in Sec. V.

## II. THE MODEL

We consider the FitzHugh–Nagumo model for two scalar fields $u$ and $v$:

$$\frac{\partial u}{\partial t} = -\frac{u^3}{3} + u - v + D_u \nabla^2 u,$$
$$\frac{\partial v}{\partial t} = \epsilon(u - \alpha v + \beta) + D_v \nabla^2 v. \tag{1}$$

In this model $\epsilon$ is the ratio of the time scales associated with the two fields and $D_u$ and $D_v$ are the constant diffusion coefficients. The parameters $\alpha$ and $\beta$ characterize the local dynamics. In this paper we concentrate on the excitable regime and take $0<\epsilon<1$.

We solve Eq. (1) numerically using an algorithm that automatically adjusts the time step to achieve an efficient simulation while controlling the error in the solution.[14] The reaction medium is a spherical shell whose outer and inner radii we denote by $R_e$ and $R_i$, respectively. Any point in the medium can be unambiguously defined by the usual set of spherical coordinates $\rho \in [R_i, R_e]$, $\theta \in [0, 2\pi]$, and $\phi \in [0, \pi]$.

The initial condition was taken to be a domain of excited state,

$$\{\rho, \theta, \phi : R_i \leq \rho \leq R_e, \theta_0 \leq \theta \leq \theta_0 + \Delta\theta, \phi_0 \leq \phi \leq \phi_0 + \Delta\phi\}, \tag{2}$$

adjacent to a domain of the refractory state,

$$\{\rho, \theta, \phi : R_i \leq \rho \leq R_e, \theta_0 - \Delta\theta \leq \theta < \theta_0, \phi_0 < \phi \leq \phi_0 + \Delta\phi\}. \tag{3}$$

This initial condition produces a pair of counter-rotating spiral waves. Observing the outer surface of the shell, one sees the formation of two spiral wave tips: one located at $\theta = \theta_0$ and $\phi = \phi_0$ and the other at $\theta = \theta_0$ and $\phi = \phi_0 + \Delta\phi$. They extend inwards forming two straight filaments connecting the inner and outer surfaces of the spherical shell.

Since the dynamics are locally periodic and the phase space trajectory is a closed loop, it is possible to introduce a phase variable $\Phi(\mathbf{r}, t) = \arctan(v(\mathbf{r}, t)/u(\mathbf{r}, t))$ which parametrizes the trajectory. A phase map $\mathcal{M}$ associates to each point in a well-defined two-dimensional domain $\mathcal{D}$ a phase lying on the unit circle, $\Phi \in S^1$. Suppose the domain is the surface of a sphere. Consider any closed curve, $C \in \mathcal{D}$, not passing through singularities of the phase map. The index $I$ of $C$ is defined in the following way. As $C$ is traversed once in a clockwise orientation, we compute

$$2\pi I = \oint_C \nabla\Phi \cdot d\mathbf{l}. \tag{4}$$

By continuity, $I$ must be an integer. The index of a singular point is defined by drawing a small circle $A$ around the singular point that contains no other singular points. The index or topological charge of the singular point is equal to the index of $A$. The following results may be deduced from this construction. The index of any closed curve $C$ not passing through any singularities is equal to the sum of the indices of the singular points contained in $C$. The sum of the indices of the singular points of a two-dimensional medium with periodic boundary conditions is invariant.[15] Further, for a closed oriented two-dimensional manifold, the sum of the indices of all singular points is equal to zero.[16] If the medium is three dimensional, the arguments apply to every two-dimensional surface bounded only by $C$.[17] These results place constraints on the dynamics of the filaments discussed in the following sections. In particular, on the surface of the sphere, spirals appear as pairs, one with index $+1$ and the other with index $-1$, so that the net index of each pair is 0. In other contexts, singularities in phase maps have been called defects[18] and the index is sometimes called the topological charge.[19]

In order to investigate the effect of geometry on the evolution of the spiral scroll waves, various values of the outer radius, $R_e$ and thickness $\Delta = R_e - R_i$ were considered. We have chosen the initial conditions such that one tip forms near one of the poles and the other on the equator, i.e., $\phi_0 = 0$, $\Delta\phi = \pi/4$, and $\Delta\theta = 10°$. For small values of the thickness the filaments remain attached to the inner and outer surfaces of the spherical shell for all times and the system behaves essentially as a two-dimensional surface: the scroll wave dynamics are similar to that of spiral waves on a spherical surface.[11] An instantaneous picture of a scroll wave in a thin spherical shell is shown in Fig. 1(a). In this case the excitation pattern on the outer surface matches that on the inner surface.

Keeping the outer radius fixed while increasing the thickness, the scroll wave filaments remain attached to the inner and outer surfaces of the spherical shell until a critical inner radius, $R_i(\min)$, is reached at which point an important qualitative change is observed. For $R_i < R_i(\min)$, after some transient time, the two filaments collide and merge to form a single curved filament. In certain parameter ranges this single filament shrinks and finally disappears. An instantaneous picture of such a scroll wave is shown in Fig. 1(b). Thus, under these conditions the scroll wave pattern is desta-

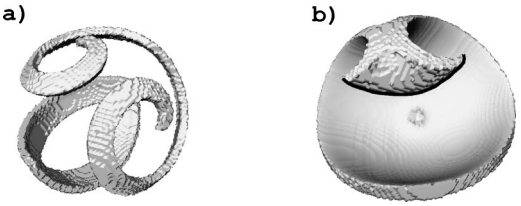


FIG. 1. Scroll wave pair in a spherical shell. System parameters: $\alpha=0.2$, $\beta=0.75$, $\epsilon=0.2$, $D_u=2$, and $D_v=0$. (a) Thin shell: $R_i \gg R_i(\min)$, and (b) thick shell, $R_i < R_i(\min)$. In this figure (and in Figs. 3 and 5) isosurfaces $0 \leqslant \Phi(\mathbf{r},t) \leqslant \Phi^*$ are shown, where the threshold $\Phi^*$ was chosen to display the essential features of the scroll waves. In panel (b) the curved filament connecting the two spiral tips on the outer surface of the spherical shell is shown as a thick line. Also in this panel, the small circular region in the center corresponds to the inner surface of the spherical shell.

bilized by a factor entirely dependent on the geometry of the medium. It is the inability of the inner surface to accommodate the scroll wave dynamics that is responsible for the destabilization of the pattern.

For the set of parameters employed here, the value of the critical radius was found to be $R_i(\min)=9$ and independent of the value of the outer radius, as shown in Fig. 2, where the line marking the transition from persistent to transient spirals is parallel to the bisectrix (the line corresponding to $R_i=0$). Transient scroll waves of the form in Fig. 1(b) are found in the region "T," while persistent spirals of the form of Fig. 1(a) are found in region "P." We study thin spherical shells in Sec. III and thick spherical shells in Sec. IV.

## III. THIN SPHERICAL SHELL

In this section we focus on the properties of scroll waves in thin spherical shells with $R_e-R_i=2$ where the scroll waves behave as spiral waves on the surface of a sphere with radius $R_e$.

### A. Minimum spherical shell size

There is a critical size of the thin spherical shell below which self-sustained spiral waves cannot exist. From purely geometric considerations this critical size $R_m$ can be related to the spiral wavelength $\lambda$. This problem has been considered earlier in the context of spiral waves in cardiac tissue.[20] For the set of parameters chosen in our simulations the radius of the smallest sphere that still supports spirals is $R_m=10$.

A rough estimate of $R_m$ can be obtained in the following way: Monitoring the local dynamics at fixed spatial points on the spherical surface, one may determine the rotation period of the pattern, $\tau$. The wave propagation velocity, $c_p$, was calculated from the times of excitation of two spatial points separated by a known fixed distance. The wavelength is then $\lambda=\tau c_p$ and $R_m$ can be estimated from the condition $2\pi R_m/\lambda \approx 1$, i.e., when the wavelength is of the same order of magnitude as the perimeter.

Simulations show that $\tau \approx 17$ time units and that it varies only very slightly with $R_e$ in the interval investigated, $12 \leqslant R_e \leqslant 68$. The wavelength $\lambda \approx 38$ space units and its dependence on $R_e$ was also found to be very weak. For large spheres the ratio $\mathcal{R}=2\pi R_e/\lambda$ is large and there is enough surface to sustain the spiral wave dynamics. However, as the radius decreases the denominator of this expression changes much more slowly than the numerator and $\mathcal{R}$ decreases. In our simulations we found that spiral waves cannot be sustained for $\mathcal{R}<1.6$, in reasonable agreement with the crude estimate of the critical value given above. It may be possible to construct more accurate estimates for the critical radius using properties of the spiral core like its size and the effective range of core–core interactions.

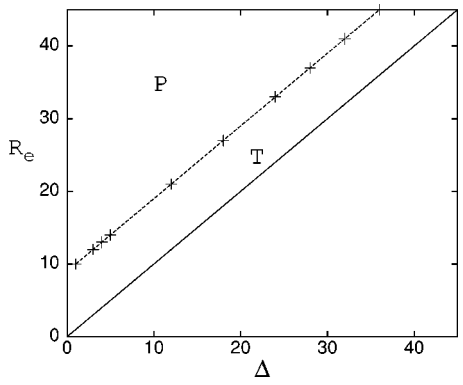


FIG. 2. Regions of existence of persistent and transient spirals separated by the transition line denoted by crosses. The solid line is the line $R_i=0$. Permanent spirals exist in region P while transient spirals exist in region T. The patterns observed in each of these regions correspond to those of Figs. 1(a) and 1(b), respectively.

### B. Regular distribution of many spirals

We now consider the number of spirals that can fit on a spherical surface with a given radius $R_e$. To study this problem we use a particular class of initial conditions: a regular arrangement of $p$ domains of excited and refractory regions of the type considered in Eqs. (2) and (3). The spiral tips are initially located on opposite poles of the sphere and the excited and refractory regions positioned so that all spirals propagate in the same direction. The angular separation between two consecutive domains in this regular arrangement is $2\pi/p$. We describe now what is observed for different numbers of initial spiral pairs, $p$, on a thin shell ($R_e-R_i=2$) with $R_e=44$.

For $p \leqslant 7$ all tips recede from the poles and stabilize at an angle $\phi_s(p)$ with respect to a line passing through the poles. The resulting pattern consists of $p$ equivalent spiral wave pairs that propagate on the spherical surface. A qualitative change in behavior occurs for $p=8$. The resulting stable pattern is shown in Fig. 3. The system rapidly evolves into a pattern of alternating long and short spiral pairs. The spiral tips are distributed in a set of two different $\phi_s(8)$ angles. This state is very sensitive: small deviations from the regular angular separation in the initial condition rapidly lead to the annihilation of some of the pairs.

For the parameters considered here, the maximum number of spiral pairs that is stable under this configuration is eight. For $8<p<13$ the system evolves into a pattern with seven or fewer spiral pairs. For instance, a pattern with 12 initial spiral pairs evolves to a pattern with eight pairs and finally to a stable pattern with four spiral pairs. A pattern with 13 initial spiral pairs quickly evolves to a completely

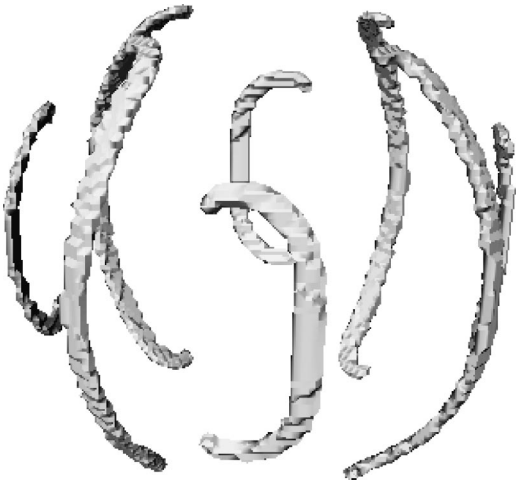

FIG. 3. Phase isosurfaces at one time instant showing a regular distribution of eight spirals in the thin spherical shell with alternating short and long spiral pairs.

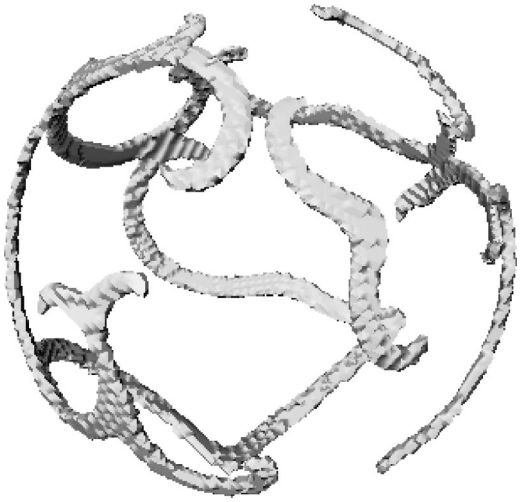

FIG. 5. Instantaneous picture of the phase isosurfaces for a system where 20 spiral pairs were randomly initiated.

quiescent state by annihilation of all spiral pairs. The angle $\phi_s(p)$ versus $p$ is shown in Fig. 4.

### C. Random distribution of many spirals

In addition to regular distributions of initial spiral pairs, we have considered random distributions where the initial-condition domains used to generate spiral pairs are randomly distributed on the surface of the sphere. We again take $R_e = 44$ and $\Delta = 2$. The random initial condition was generated in the following way: the tips of the initial-condition domains are taken to have $\phi$ and $\theta$ values uniformly distributed on $0 < \phi < \pi/2$ and $0 < \theta < 2\pi$, respectively. After such a domain is chosen, a rigid-body rotation of the domain was performed with Euler angles chosen randomly. This procedure was repeated for each of the $p$ initial spiral pairs with no attempt to avoid overlap of the initial-condition domains.

During the evolution from the initial state, pairs of singularities with index $+1$ and $-1$ may annihilate or new pairs of singularities may form as a result of breaking of wave fronts. As a result a complicated pattern of spiral wave pairs can form on the sphere (see Fig. 5).

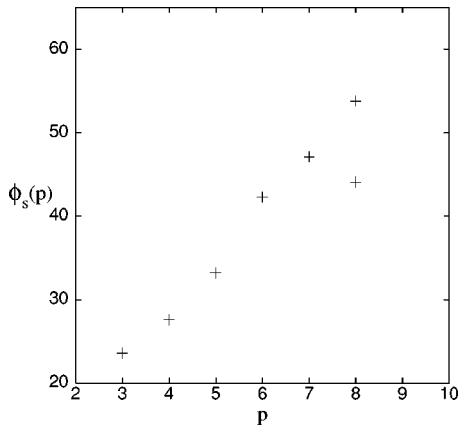


FIG. 4. The angle $\phi_s(p)$ versus $p$. The maximum number of stable spiral pairs is $p = 8$ for which there are two different angles.

As a result of annihilation and creation events the number of singularities in the system may vary with time but for this parameter value any realization of the evolution from the random initial condition evolves to a state with a fixed number of singularities. We define $n_s(\infty)$ to be the average number of singularities which survive starting from an initial configuration with $n_s(0) = 2p$ singularities. A plot of $n_s(\infty)$ versus $n_s(0)$ is shown in Fig. 6.

When the initial number of singularities is small, $n_s(\infty) \approx n_s(0)$ since most of the initially formed spiral pairs are likely to survive. However, $n_s(\infty)$ saturates for large $n_s(0) > 40$ due to the annihilation of closely spaced defect pairs. From the figure we may estimate this saturation value to be $n_s(\infty) \equiv n_s^* \approx 17.55 \pm 3.22$. Thus, the average maximum number of randomly distributed spiral pairs that can fit on a sphere with $R_e = 44$ is about nine, which is very close to the value of eight obtained for a regular initial configuration.

From these results we may estimate the maximum average density of spiral waves on the sphere as $\rho_s^*$

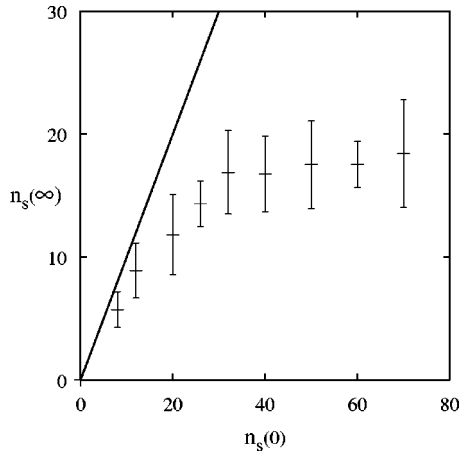


FIG. 6. Number of surviving singularities $n_s(\infty)$ as a function of the initial number $n_s(0)$ for a spherical shell with $R_e = 44$ and $R_i = 42$. Each point is the average of 14 realizations and the vertical bars have length of twice the standard deviation. The solid is the bisectrix.

$=n_s^*/4\pi R_i^2$, where we have used $R_i$ since the inner surface of the thin spherical shell is smaller. For the spherical shell with $R_i=42$ we find $\rho_s^*=7.9\times10^{-4}$. If the spiral density is constant for a fixed set of parameter values, one may then determine the maximum average number of spiral waves on a sphere of any size. For example, we predict that a spherical shell with $R_i=28$ will support, on average, a maximum of eight ($n_s^*=4\pi R_i^2\rho_s^*=7.8$) spiral waves, while simulations show that $n_s^*=8.15\pm3.0$.

One may use $\rho_s^*$ even to estimate the size of a sphere that will support a single spiral wave pair, $R_{\min}=(\rho_s^*\pi)^{-1/2}$. Taking the above value of $\rho_s^*$ we find $R_{\min}=14.2$, which is comparable to but somewhat larger than the value of $R_{\min}=10$ found in Sec. III A.

## IV. SCROLL WAVES IN A THICK SPHERICAL SHELL

### A. Scroll wave dynamics

The filament of the scroll wave is a space curve which can be described by a parametric equation $\mathbf{R}(t,s)=(x(t,s),y(t,s),z(t,s))$ where $t$ is the time and $s$ is the arc length, $0\leqslant s\leqslant L(t)$ with $L(t)$ the total length of the filament. An orthogonal coordinate system can be attached to each point of the curve with tangent $\mathbf{t}(s)$, normal $\mathbf{n}(s)$, and binormal $\mathbf{b}(s)$ unit vectors defined by

$$\mathbf{t}(s)=\frac{d\mathbf{R}}{ds},\quad \mathbf{n}(s)=\frac{d\mathbf{t}/ds}{|d\mathbf{t}/ds|},\quad \mathbf{b}(s)=\mathbf{t}(s)\times\mathbf{n}(s). \tag{5}$$

A full description of a scroll wave requires a specification of the local phase or "twist."[21] This is accomplished in the following manner. In the plane normal to the filament (spanned by $\mathbf{n}$ and $\mathbf{b}$), the scroll wave appears as a two-dimensional spiral rotating around the point where the filament pierces the plane. The local phase of the spiral can be defined as the angle between some unit vector $\mathbf{V}$, rotating rigidly with the spiral and some local reference direction. Choosing $\mathbf{V}=\mathbf{n}\cos\phi+\mathbf{b}\sin\phi$, where $\phi$ is the angle $\mathbf{V}$ makes with the normal, $\mathbf{n}$, we may write the local twist rate as

$$w(s)=\frac{d\mathbf{V}}{ds}\cdot\mathbf{t}\times\mathbf{V}=\tau(s)+\frac{d\phi}{ds}, \tag{6}$$

where $\tau(s)$ is the torsion, $\tau(s)=|d\mathbf{b}/ds|$.

Theoretical investigations of the dynamics of three-dimensional scroll waves with a filament of arbitrary shape were carried out by Keener[22] who derived its equation of motion. For an untwisted filament in a plane his equations reduce to

$$\frac{d\phi}{dt}=a\kappa,\quad \frac{d\mathbf{R}}{dt}\cdot\mathbf{b}=b\kappa,\quad \frac{d\mathbf{R}}{dt}\cdot\mathbf{n}=c\kappa, \tag{7}$$

where $\kappa=|d\mathbf{t}/ds|$ is the curvature and the coefficients $a$, $b$, and $c$ can be determined from a knowledge of the eigenvalue problem corresponding to the linearized reaction–diffusion equation. In general, at any moment of time the motion of the filament has three components: (a) a component in the direction of the normal unit vector, $d\mathbf{R}(t,s)/dt\,\mathbf{n}$, or "shrinking," (b) a component in the direction of the binormal unit vector, $d\mathbf{R}(t,s)/dt\,\mathbf{b}$, or "drifting," and (c) a meandering motion.

A simplification of the dynamics occurs when $D_u=D_v=D$. In this case, $c=D$ and $a=b=0$. A planar filament remains in the same plane at all times and the normal velocity is proportional to the diffusion coefficient. This law has been confirmed experimentally in the context of spirals in Belousov–Zhabotinsky reagent.[23] In the more general case of unequal diffusion coefficients, $b$ is not zero, and a planar filament will not remain planar unless the filament is initially exactly a circle. Similarly, if $a$ is not zero an untwisted filament will develop twist as time proceeds unless it is exactly circular initially.[22]

We now describe the behavior of a scroll wave in a system where the internal radius is below the critical value $R_i(\min)$ so that the inner surface of the spherical shell cannot support a spiral pair. Using the initial conditions described earlier, the two straight filaments connecting the the outer and inner surfaces detach from the inner surface after some interval and merge to form a single curved filament as in Fig. 1(b). The subsequent evolution of this filament depends on the values of the parameters of the model. For values of $\beta$ for which the amplitude of the meandering is small, the filament rapidly attains the shape of an arc circle with radius of curvature $\rho(t)$ and shrinks until it disappears. For values of $\beta$ close to the meandering transition, where the amplitude of the meandering is large, the filament enters a turbulent regime; this case is studied in detail in Sec. IV E.

In the calculations reported in the remainder of this section, the internal radius was set to zero and we consider a solid sphere with $R_e=R$. Similar results obtain provided $R_i<R_i(\min)$, well into the transient region of Fig. 2. We consider initial conditions that generate spiral pairs whose tips are located on opposite poles of the sphere; i.e., initially the filament is a straight line passing through the center of the sphere. We choose the Cartesian axes so that initially the filament runs along the $z$ axis and the center of the sphere is the origin of the Cartesian coordinate system.

### B. Meandering

We have studied the meandering of the filament for various values of $\beta$. There have been many investigations of meandering in two-dimensional media (see, for instance, Ref. 1, and articles therein) and explicit calculations of the meandering "$\beta\epsilon$-phase diagram" for the FitzHugh–Nagumo system have been carried out.[24] Here we simply focus on the nature of the meandering of the filament in our three-dimensional solid sphere geometry for the selected values of $\beta$ employed in our study.

Figure 7 shows the trajectories of the intersection of the filament with the $xy$ plane, $z=0$ for three values of $\beta$ and $\epsilon=0.2$ in a solid sphere with radius $R=90$. For $\beta=0.75$, the amplitude of the meandering motion is about nine space units which is small compared to the sphere dimensions. The meander amplitude increases as $\beta$ approaches the edge of the meandering region in the $\beta\epsilon$-phase diagram. The largest meander amplitude shown in Fig. 7 corresponds to a value of

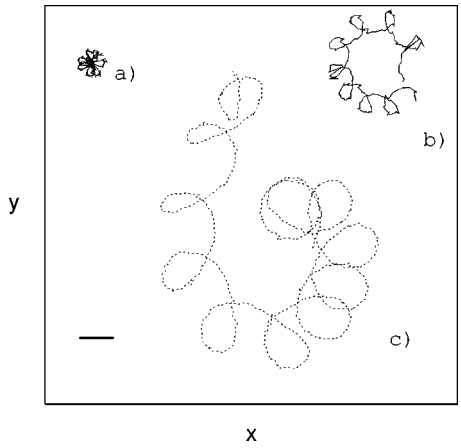


FIG. 7. Trajectories of the intersection of the filament with the plane $z=0$ for various values of $\beta$. (a) $\beta=0.75$, (b) $\beta=0.90$, and (c) $\beta=1.0$. The straight line has length 10 and is shown as reference.

$\beta=1.0$, very close to the meander border. With further change of $\beta$ three borders are crossed in succession in the following order: the meander border, the rotor border and finally the propagation border, as described by Winfree.[24] Although no attempt has been made to locate precisely these points, it was verified that for $\beta=1.05$ the system is outside the propagation region.

When the meander amplitude is small, as for $\beta=0.75$ (see Fig. 7), the effect of meander on the overall motion of the filament is not important; it simply introduces noticeable dispersion about the mean filament position. For this $\beta$ value we have found that all segments of the filament move in phase so that in this regime the filament meanders as a nearly rigid body. In the next section we discuss the shrinkage and disappearance of the filament. We note that the meandering period is about 30 time units which is small compared to the total lifetime of the filament of approximately 7200 time units. These observations suggest that meandering has little effect on the results for shrinking and drifting in these parameter values.

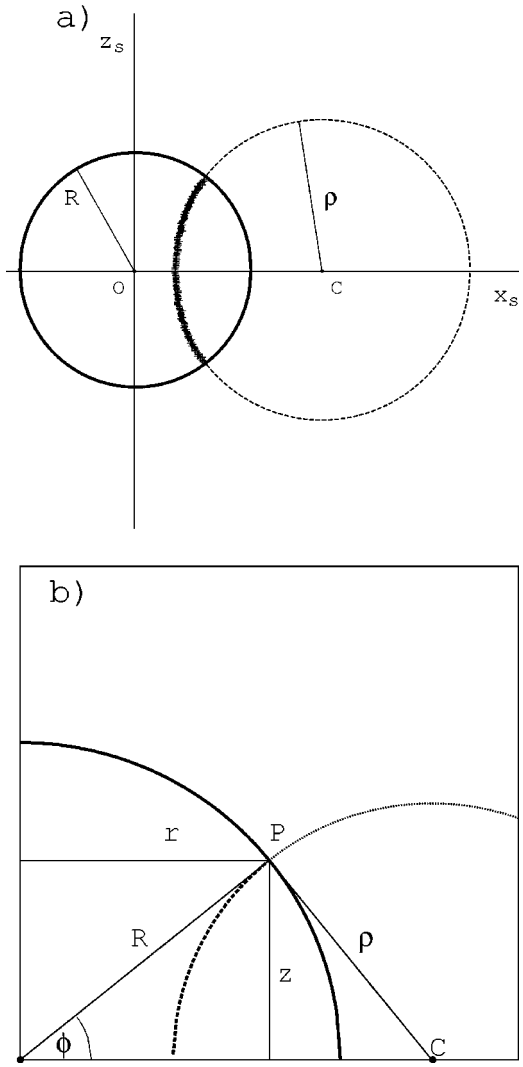


FIG. 8. (a) Fit of the filament (dense set of points) with an auxiliary circle (short dashed line) of radius $\rho(t)$. The left circle (thick black line) is a cut through the physical sphere with radius $R=90$ and center at $O$ by a plane containing the filament. (b) Detail showing the intersection of the filament with the sphere surface, point $P$.

### C. Shrinking

Starting with an initially straight filament passing through the poles of the sphere, for $\beta=0.75$, after some transient time, the filament adopts the shape of an arc of a circle and maintains this shape as it shrinks. Since the filament tangent vector **t** at the surface of the sphere is normal to the sphere surface, one can readily calculate the radius of curvature of the filament at any time. We have done this for two different sphere radii, $R=90$ and 45. Figure 8(a) shows a cross section of the physical sphere taken in the plane in which the filament lies, as well as an auxiliary circle that fits the filament and from which we may extract the radius of curvature. The filament is taken to lie in the $x_s z_s$ plane. Since initially the filament lies on the sphere $z$ axis and remains parallel to this axis at all times, the plane of the filament is always perpendicular to the $xy$ plane and the $z_s$ and $z$ axes always coincide.

We may use Eqs. (7) to derive equations for the time evolution of the filament. The calculation is easier for the intersection point $P$ in Fig. 8 of the filament with the surface where various simple trigonometric relations apply. Figure 8(b) shows the geometry at some particular time $t$ in the plane of the filament. The thick black line represents the physical sphere of radius $R$ and the dotted line is a sketch of the filament at that particular time. Let $r$ denote the distance of the tip of the filament to the $z$ axis. It is easy to see that

$$\rho=\frac{R}{r}\sqrt{R^2-r^2}=\frac{Rz}{r}. \tag{8}$$

Applying Eqs. (7), point $P$ moves in the direction of the normal **n** (tangent to the surface) with speed

$$v_n=c\kappa=\frac{c}{\rho}. \tag{9}$$

The horizontal component of this velocity is

$$v_{n,r}=v_n\sin\phi=\frac{v_n z}{R}, \tag{10}$$

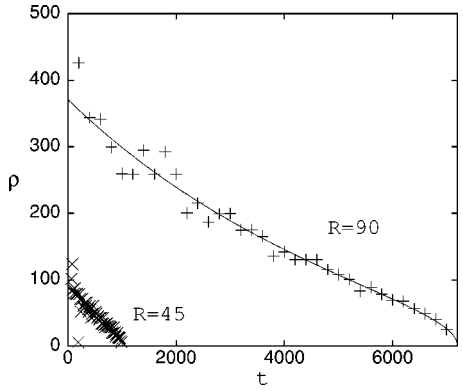


FIG. 9. Time evolution of the radius of curvature of the filament. Pluses are values from the simulation in a sphere with $R=90$ while crosses are for $R=45$. The solid lines are calculated using Eq. (14) with $c=6.5$.

where the angle $\phi$ is defined in Fig. 8. Substitution of Eqs. (9) and (8) yields a differential equation for $r$,

$$v_{n,r}=\frac{dr}{dt}=\frac{c}{R^2}r, \tag{11}$$

which can be readily solved to give

$$r(t)=r(0)e^{ct/R^2}. \tag{12}$$

This equation can be expressed in terms of the lifetime $t_f$ by noticing that $r(t_f)=R$. Thus,

$$r(t)=Re^{c(t-t_f)/R^2}. \tag{13}$$

Finally, substituting into Eq. (8) we obtain

$$\rho(t)=R(e^{2c(t_f-t)/R^2}-1)^{1/2}. \tag{14}$$

From this equation, other features, such as the length of the filament, $L$, can be calculated. We have

$$L(t)=2R(e^{2c(t_f-t)/R^2}-1)^{1/2}\arcsin(e^{c(t-t_f)/R^2}). \tag{15}$$

The results are shown in Figs. 9 and 10, where it can be seen that the agreement with the numerical simulation is excellent. Equations (14) and (15) should be used only after a transient time when the filament adopts the shape of an arc of a circle.

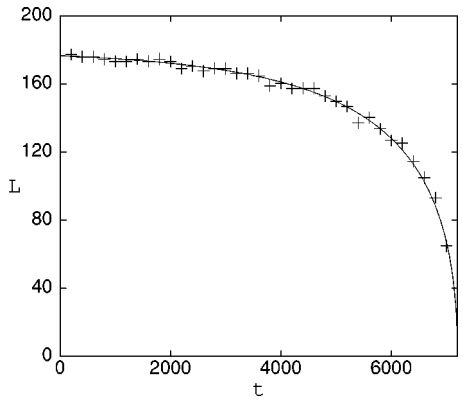


FIG. 10. Time evolution of the length of the filament. Pluses are values from the simulation in a sphere with $R=90$ and the solid line is the length from Eq. (15) with $c=6.5$.

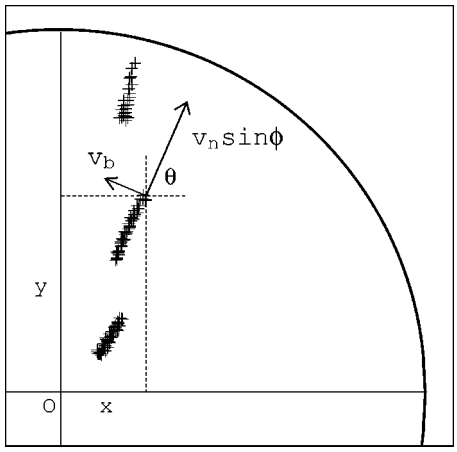


FIG. 11. Projection of the system on the $xy$ plane. The thick line is the perimeter of the physical sphere. Pluses indicate the filament at three different times, from bottom to top, $t=350,1200,1750$.

### D. Drifting

Lateral drifting of scroll rings has been observed when the diffusion coefficients are unequal[25,26] as is the case in this work. However, the presence of a spherical surface introduces an important qualitative difference. Because of the curvature of the surface at which both tips of the filament are attached, the binormal component of the filament results in a slow rotation of the filament plane around the axis of symmetry of the sphere. The situation is illustrated in Fig. 11 where the projection of the filament on the $xy$ plane is shown for three different times. The plane of this figure is perpendicular to that of Fig. 8.

The rotation of the filament plane can be described by an angle $\theta$ with respect to an arbitrary axis. As shown in Fig. 8(b), the intersection of the filament with the sphere is located at point $P$ at a distance $r$ from the $z$ axis. The analysis is similar to that for the shrinkage of the filament, but in this case both proportionality constants, $b$ and $c$ in Eq. (7), enter the equation of motion. From Figs. 8 and 11 the component of the velocity vector in the direction of the $x$ axis is

$$\frac{dx}{dt}=v_x=v_n\cos\theta\sin\phi-v_b\sin\theta$$

$$=\frac{c\sqrt{R^2-r^2}}{\rho r}\cos\theta-\frac{b}{\rho}\sin\theta. \tag{16}$$

Using $dx/dt=(dr/dt)\cos\theta-r\sin\theta(d\theta/dt)$ and Eq. (8), we obtain a differential equation for $\theta$,

$$\frac{d\theta}{dt}=\frac{b}{R\sqrt{R^2-r^2}}=\frac{b}{R^2\sqrt{1-e^{2c(t-t_f)/R^2}}}. \tag{17}$$

This equation can be integrated to obtain

$$\theta(t)=\theta(0)+\frac{b}{R^2}t+\frac{b}{c}\ln\frac{1+\sqrt{1-e^{-2ct_f/R^2}}}{1+\sqrt{1-e^{2c(t-t_f)/R^2}}}. \tag{18}$$

Results from this equation are compared to those from the numerical simulation in Fig. 12 and the agreement is very good. We have found that the drifting velocity is small com-

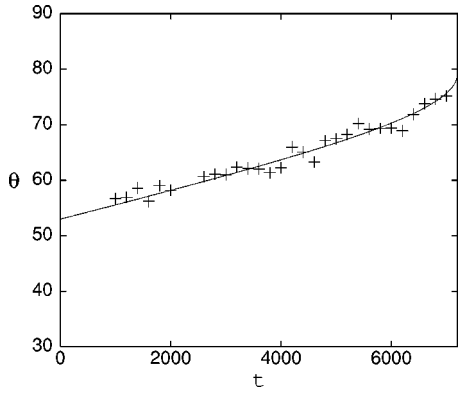


FIG. 12. Time evolution of the angle of the filament plane with respect to an arbitrary axis. Pluses are results from the simulation and the solid line is the solution of Eq. (18) with $b=1.45$.

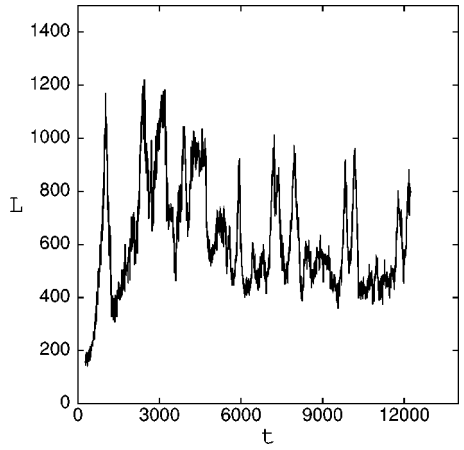


FIG. 14. Time evolution of the total length of the filament segments in the turbulent regime.

pared to the shrinking velocity. With the choice of parameters made here, $c/b \approx 4.5$. Furthermore, Eq. (18) shows that at early times the rotation rate is dominated by the linear term $bt/R^2$ which is small for large spheres. Indeed, in our case the plane of the filament rotates only about 24° before vanishing.

### E. Turbulent regime

For values of $\beta$ close to the meander border, the filament neither shrinks nor remains planar as described in the preceding section but instead its dynamics becomes turbulent. The elongation and bending of the initially straight filament is shown in Fig 13. In this parameter regime, the filament continues to stretch and bend until a segment of the filament collides with the surface of the sphere. At this point the filament breaks into new shorter filaments whose dynamics, in turn, follow the same pattern. Through this process many filament segments with different lengths are created. If the resulting filament segments are too small they shrink and disappear.

Figure 14 shows the time evolution of the total length of the filament segments. After a long transient period, the length attains a constant average value about which there are large fluctuations. Major filament annihilation events occur when the newly formed filament segments are so small that they disappear soon after their formation. In addition to shrinkage of small filament segments, in this turbulent regime we have observed occasionally the formation of expanding scroll rings. Expanding scroll rings near the meandering transition have been observed earlier.[25,27] Equations (7) support expanding scroll rings if the coefficient $b$ is negative, which may occur if the diffusion coefficients are not equal.[22]

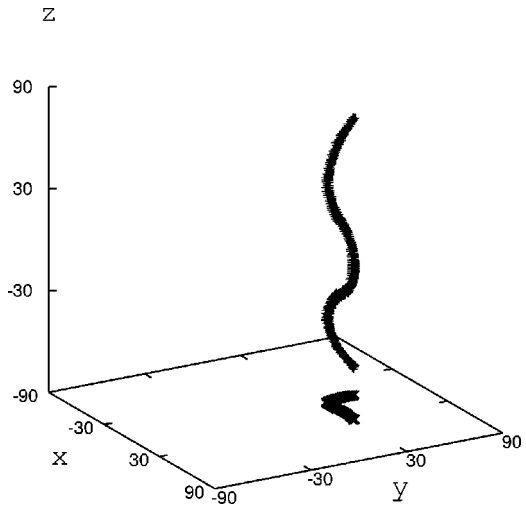


FIG. 13. Instantaneous configuration of the filament in the region close to the meandering transition, $\beta=1.0$.

Since turbulent filament dynamics occur throughout the spherical volume, if the radius of the sphere is large enough the surface to volume ratio will be small and the character of the filament turbulence is expected to be similar for different geometries. However, for smaller spheres the dynamics of filaments which are connected to the surface will play a significant role and we expect that the turbulent evolution will depend on the geometry. To fully investigate this problem studies of filament turbulence as a function of sphere size must be carried out and compared with those for different geometries.

Filament instabilities have been studied in models of excitable media[28] and in models of anisotropic cardiac tissue.[29] Filament turbulence has also been observed in the complex Ginzberg–Landau equation.[30]

## V. DISCUSSION

For thin spherical shells the vortex filaments remain attached to the inner and outer surfaces. In this quasi-two-dimensional case the mean number of spiral pairs that a sphere with given radius can support may be determined. For thick spherical shells the filaments may detach from the smaller inner surface and the resulting dynamics may result either in simple shrinkage or in turbulent filament dynamics, depending on the system parameters.

Part of the motivation for the present study stems from the application of such scroll wave dynamics to the physiology of cardiac arrhythmias. Although a real heart is inhomogeneous and has a very complicated geometry and local dy-

namics, the problems studied in this paper are also of relevance for the heart. In particular, scroll waves are believed to play a role when the heart is in fibrillation or exhibits flutter. It is then important to determine how many spiral waves the heart can support and to characterize their dynamics. The observation that scroll waves are only sustained in a spherical shell of certain minimum size is consistent with the finding that a critical mass is essential to sustain ventricular fibrillation in a mammalian heart.[31]

While the topology of a real heart is quite complex and differs from that of a simple spherical shell due to the ''holes'' arising from valves and veins, some of the principal features of scroll wave dynamics are best elucidated by studying more simple dynamics in simple geometries, such as the spherical shell considered here. One may build on the understanding of the dynamics presented here by extending such simple models to include more complicated features, such as holes, varying shell thickness, or inhomogenieties.

## ACKNOWLEDGMENT

This work was supported in part by a grant from the Canadian Network of Centers of Excellence on Mathematics of Information Technology and Complex Systems (MITACS).

[1] *Chemical Waves and Patterns*, edited by R. Kapral and K. Showalter (Kluwer, Dordrecht, 1994).
[2] A. Goldbeter, *Biochemical Oscillations and Cellular Rhythms* (Cambridge University Press, Cambridge, 1996).
[3] A. T. Winfree, *When Time Breaks Down* (Princeton University Press, Princeton, NJ, 1987).
[4] *Computational Biology of the Heart*, edited by A. V. Panfilov and A. V. Holden (Wiley, Chichester, 1997).
[5] *Cardiac Electrophysiology: From Cell to Bedside*, edited by D. P. Zipes and J. Jalife (W. B. Saunders, Philadelphia, 1995).
[6] J. Jalife, R. A. Gray, and G. E. Morley, Chaos **8**, 79 (1998).
[7] P. Grindrod and J. Gomatam, J. Math. Biol. **25**, 597 (1987).
[8] P. K. Brazhnik, V. A. Davydov, and A. S. Mikhailov, Theor. Math. Phys. **74**, 440 (1988).
[9] V. A. Davydov and V. S. Zykov, Physica D **49**, 71 (1994).
[10] P. McQuillan and J. Gomatam, J. Phys. Chem. **100**, 5157 (1996).
[11] J. Gomatam and F. Amdjadi, Phys. Rev. E **56**, 3913 (1997).
[12] H. Yagisita, M. Mimura, and M. Yamada, Physica D **124**, 126 (1998).
[13] J. Maselko and K. Showalter, Nature (London) **339**, 609 (1989).
[14] G. Rousseau and R. Kapral, Chaos **10**, 812 (2000).
[15] Y. Kuramoto, *Chemical Oscillations, Waves and Turbulence* (Springer, Berlin, Heidelberg, 1984).
[16] L. Glass, Science **198**, 321 (1977).
[17] A. T. Winfree and S. H. Strogatz, Physica D **8**, 35 (1982).
[18] N. D. Mermin, Rev. Mod. Phys. **51**, 591 (1979).
[19] A. S. Mikhailov, *Foundations of Synergetics I: Distributed Active Systems* (Springer-Verlag, New York, 1994).
[20] G. E. Morley, F. H. Samie, and J. Jalife, J. Am. Coll. Cardiol. **29**, 330 A (1997); G. Salama, A. Kanai, and I. R. Efimov, Circulation Res. **74**, 604 (1994).
[21] M. Tabor and I. Klapper, Nonlinear Sci. Today **4**, 7 (1994); **4**, 12 (1994).
[22] J. P. Keener, Physica D **31**, 269 (1988).
[23] J. P. Keener and J. J. Tyson, Science **239**, 1284 (1988).
[24] A. T. Winfree, Chaos **1**, 303 (1991).
[25] A. V. Panfilov and A. N. Rudenko, Physica D **28**, 215 (1987).
[26] M. Courtemanche, W. Skaggs, and A. T. Winfree, Physica D **41**, 173 (1990).
[27] A. T. Winfree, SIAM Rev. **32**, 1 (1990), and references therein.
[28] Z. Qu, F. Xie, and A. Garfinkel, Phys. Rev. Lett. **83**, 2668 (1998).
[29] W.-J. Rappel, Chaos **11**, 71 (2001).
[30] I. S. Aranson, A. R. Bishop, and L. Kramer, Phys. Rev. E **57**, 5276 (1998).
[31] A. T. Winfree, Science **266**, 1003 (1994).